Non-Fermi-liquid behavior of the scattering rate in the three-orbital Emery model

Tianzong Mao [1] and Mi Jiang [1,2]

[1] *School of Physical Science and Technology, Soochow University, Suzhou 215006, China*

[2] *Jiangsu Key Laboratory of Frontier Material Physics and Devices, Soochow University, Suzhou 215006, China*

(Received 19 March 2024; revised 5 May 2024; accepted 15 May 2024; published 3 June 2024)

Motivated by the recent findings on the T-linear electronic scattering rate in the two-dimensional Hubbard model, we have investigated the three-orbital Emery model and its temperature-dependent electronic and quasiparticle scattering rates by adopting dynamical cluster quantum Monte Carlo simulations. By focusing on two characteristic site energies ϵ_p of O-2p orbital relevant to cuprates and nickelates separately, our exploration discovered that, for $\epsilon_p = 3.24$ relevant to cuprates, the scattering rate can exhibit a linear-T dependence at low temperature for a range of intermediate densities. In contrast, for larger $\epsilon_p = 6.0$ presumably relevant to nickelates, a wide range of densities support a downturn of the scattering rate below the temperature scale $T \sim 0.1$ with possibly two consecutive nearly linear-T regimes connected via a smooth crossover around $T \sim 0.1$. Furthermore, the temperature-dependent quasiparticle scattering rate generically departs from the unity slope as predicted by the Planckian dissipation theory. Our presented work provides valuable insights on the extensively studied three-orbital Emery model, particularly on the quantitative examination of non-Fermi-liquid features of scattering rates.

DOI: 10.1103/PhysRevB.109.245102

I. INTRODUCTION

As a central topic in condensed matter physics, non-Fermi-liquid (NFL) phenomenology is ubiquitous and has been extensively studied in a wide variety of materials [1–9]. One notable manifestation of NFL behavior is the strange metallic phase in cuprate superconductors [2,4,8,9], where a T-linear scattering rate $1/\tau \sim T$ is observed at quite a wide temperature regime [10], while the Landau Fermi-liquid theory conventionally predicts that $1/\tau \sim T^2$ in most metals at low temperatures. As an experimental mystery, the NFL features like transport properties distinct from the normal Fermi liquid have attracted much attention in the past decades [2–4]. Theoretically, the notion of Planckian dissipation, namely the universal Planckian limit on the scattering rate, has been proposed [3,11,12]. There have been numerous studies on this T-linear scattering rate and other NFL properties in the framework of two-dimensional Hubbard model [13–24]. In addition, theoretical analysis [25–30] and even ultracold atomic experiments [31] have provided much insight on these topics as well. Specifically, the recent study adopting dynamical cluster approximation demonstrated that the linear-T dependence of electronic scattering rate was discovered to occur in a limited range of doping levels for the square lattice model [23]. Interestingly, for triangular lattice, the most recent study uncovered two distinct doping regimes with different origins of T-linear behavior [24].

One significant issue in the study of unconventional superconductors (SC) is the proper minimal model that captures the essential low-energy physics. In spite of the success of the one-band Hubbard model and its variants in understanding unconventional SC, their common intrinsic assumption is that the parent compounds, which are sometimes charge-transfer insulators, e.g., cuprate SC [32], can instead be modeled as effective Mott insulators. For this single-band Hubbard model, although there is consensus on the absence of SC at hole doping $\delta = 1/8$, it is still highly debated on the existence of SC at other dopings [33–35].

Alternatively, the three-orbital Emery model [36] provides a more realistic representation of the copper oxide planes as it explicitly incorporates the Cu $d_{x^2-y^2}$ and the two ligand O-2p$_\sigma$ orbitals in a unit cell. Owing to its more degrees of freedom, the Emery model has been extensively studied with various many-body methodologies in the past decades [37–50]. Given that it provides a natural extension so that offers a more accurate depiction of cuprate SC compared to the single-band Hubbard model, it is imperative to ascertain whether it also hosts the linear-in-T behavior of the scattering rate at low temperatures. Note that due to the complexity originating from the multiorbital nature, it remains a challenge of achieving consensus on many aspects of its physics [49,51,52]. Furthermore, we believe that the three-orbital Emery model would be particularly important in light of the most recent experimental demonstration of the cupratelike electronic structure of infinite-layer nickelates [53,54] implying that in some sense the two different families of unconventional SC can be reasonably investigated in a common framework.

To this goal, we have explored the NFL behavior of the electronic scattering rate of the two-dimensional Emery model in different doping levels. The additional O degree of freedom introduces one important tuning parameter, namely the site energy ϵ_p of O-2p orbital compared to the 3d orbital ($\epsilon_d = 0$ is fixed). Considering that the recently discovered nickelate SC [55–59] has been proven to have larger charge-transfer energy $\Delta \equiv \epsilon_p - \epsilon_d$ than cuprates [60–62], we focused on two characteristic site energies ϵ_p of O-2p orbital relevant to cuprates and nickelates, respectively, to uncover its significant impact on the NFL behavior. Specifically, our simulations revealed

that, for ϵ_p relevant to cuprates, the electronic scattering rate shows linear-T dependence in a wide range of densities but the interception extrapolated to $T = 0$ are always tiny or negative. Intriguingly, the increment of ϵ_p leads to distinct behavior of the scattering rate, where there exist two consecutive temperature intervals for different slopes of linear-T behavior. Our investigation would not only deepen our understanding of the fundamental NFL features within Emery model governing the materials like cuprates but also unlock new connections between these two superconducting materials in a common theoretical framework.

II. MODEL AND METHOD

The three-orbital Emery model [36,51,52] is defined as $H = K_0 + K_{pd} + K_{pp} + V_{dd} + V_{pp}$ with

$$\begin{aligned} K_0 &= (\epsilon_d - \mu)\sum_{i\sigma} n^d_{i\sigma} + (\epsilon_p - \mu)\sum_{i\alpha\sigma} n^p_{i\alpha\sigma}, \\ K_{pd} &= \sum_{\langle ij\rangle\alpha\sigma} t^{i,j,\alpha}_{pd}(d^\dagger_{i,\sigma} p_{j,\alpha,\sigma} + p^\dagger_{j,\alpha,\sigma} d_{i,\sigma}), \\ K_{pp} &= \sum_{\langle jj'\rangle\alpha\alpha'\sigma} t^{j,j',\alpha,\alpha'}_{pp}(p^\dagger_{j,\alpha,\sigma} p_{j',\alpha',\sigma} + p^\dagger_{j',\alpha',\sigma} p_{j,\alpha,\sigma}), \\ V_{dd} &= U_{dd}\sum_i n^d_{i,\uparrow} n^d_{i,\downarrow}, \\ V_{pp} &= U_{pp}\sum_{j,\alpha} n^p_{j,\alpha,\uparrow} n^p_{j,\alpha,\downarrow}, \end{aligned} \tag{1}$$

where $d^\dagger_{i,\sigma}$ ($d_{i,\sigma}$) creates (annihilates) a hole with spin σ ($=\uparrow, \downarrow$) in $d_{x^2-y^2}$ orbital at site i; while $p^\dagger_{j,\alpha,\sigma}$ ($p_{j,\alpha,\sigma}$) creates (annihilates) a hole with spin σ ($=\uparrow, \downarrow$) in the p_α (α = x, y) orbital. $n^d_{i\sigma} = d^\dagger_{i\sigma} d_{i\sigma}$ are the number operators; $\langle . \rangle$ means a sum over nearest-neighbor orbitals. U_{dd} and U_{pp} are the strengths of the d and p onsite interactions, respectively. The chemical potential μ controls the total hole density ρ, where ϵ_d and ϵ_p are the site energies of the d and p orbitals, respectively. $t^{ij\alpha}_{pd} = t_{pd}(-1)^{\eta_{ij}}$ and $t^{jj'\alpha\alpha'}_{pp} = t_{pp}(-1)^{\beta_{jj'}}$ are the nearest-neighbor d-p and p-p hopping integrals. In the hole language, η_{ij} and $\beta_{jj'}$ take values ± 1 following the conventions. In hole language, the phase convention is $\eta_{ij} = 1$ for $j = i + \frac{1}{2}x, \alpha = x$ or $j = i - \frac{1}{2}y, \alpha = y$ and $\eta_{ij} = 0$ for $j = i - \frac{1}{2}x, \alpha = x$ or $j = i + \frac{1}{2}y, \alpha = y$. In addition, $\beta_{jj'} = 1$ for $j' = j - \frac{1}{2}x - \frac{1}{2}y$ or $j' = j + \frac{1}{2}x + \frac{1}{2}y$ and $\beta_{jj'} = 0$ for for $j' = j - \frac{1}{2}x + \frac{1}{2}y$ or $j' = j + \frac{1}{2}x - \frac{1}{2}y$, $\alpha = x$ and $\alpha' = y$ or $\alpha = y$ and $\alpha' = x$, respectively. Other conventions are also applicable due to the gauge invariance [51]. Unless otherwise stated, we use the parameters listed below (in units of eV): $U_{dd} = 7.5$, $U_{pp} = 0$, $t_{pd} = 1.13$, $t_{pp} = 0.49$, $\epsilon_d = 0$. Note that we do not adopt $U_{dd} = 8.5$ in the literature to alleviate the sign problem in our simulations with large dynamical cluster approximation (DCA) cluster $N_c = 16$, which should not qualitatively modify our results presented here.

In this work, we have endeavored to solve the two-dimensional three-orbital Emery model at low temperatures using the dynamical cluster approximation [63–65] with the continuous-time auxiliary-field (CT-AUX) quantum Monte Carlo (QMC) cluster solver [66]. As an advanced quantum many-body numerical method, DCA evaluates the physical quantities in the thermodynamic limit via mapping the bulk lattice problem onto a finite cluster embedded in a mean-field bath in a self-consistent manner [63,64], which is realized by the convergence between the cluster and coarse-grained (averaged over a patch of the Brillouin zone around a specific cluster momentum $\mathbf{K}$) single-particle Green's functions. In particular, the short-range interactions within the cluster are treated exactly with various numerical techniques, e.g., CT-AUX used in the present study; while the longer-ranged physics is approximated by a mean field. Therefore, increasing the cluster size systematically approaches the exact result in the thermodynamic limit. The finite size of the cluster is essentially approximating the whole Brillouin zone by a discrete set of $\mathbf{K}$ points so that the self-energy $\Sigma(\mathbf{K}, i\omega_n)$ is a constant function within the patch around a particular $\mathbf{K}$ and a step function in the whole Brillouin zone. Generically, the quantum embedding methods including DCA have better minus sign problems than the finite-size QMC simulations. More discussions on DCA technique and its insight on the strongly correlated electronic systems can be found in Ref. [64].

Our focused physical quantity is the electronic scattering rate $\gamma_k \equiv -\mathrm{Im}\Sigma^{(m)}(\mathbf{K}, \omega = 0)$. Precisely, for a desired $\mathbf{K}$, we fit the imaginary part of self-energy $-\mathrm{Im}\Sigma(\mathbf{K}, i\omega_n)$ at a few lowest Matsubara frequencies, e.g., $n = 0, 1, 2....$ to an mth order polynomial function of $i\omega_n$ and then extrapolate this polynomial to $\omega = 0$. Although the m value and largest n can affect the extrapolation generically, our results show qualitatively similar trend of T dependence of γ_k at low temperatures for different m and n values (not shown). Hence, the conventional $m = 2$ at the lowest three ($n = 0, 1, 2$) Matsubara frequencies are chosen for the extrapolation analysis [23,24]. Note that, as an approximation avoiding the ambiguous and challenging analytical continuation procedure, the accuracy of this extrapolation for zero frequency improves at low temperatures where the Matsubara frequencies are closer. In addition to the electronic scattering rate γ_k, we have further investigated the quasiparticle scattering rate or inverse quasiparticle lifetime $1/\tau_k = Z_k\gamma_k$, which incorporates the quasiparticle weight Z_k. Note that both these quantities are only the approximations of the resistivity obtained in the transport experiments manifesting the strange metal behavior. In fact, the quasiparticle picture can even break down in the strange metals [67–69]. Nonetheless, as important physical quantities that can be evaluated efficiently in our numerical DCA technique, they still provide valuable information on the intrinsic physics of the Emery model.

Most of our calculations were conducted with $N_c = 16$ sites DCA cluster for fine enough but still computationally manageable momentum-space resolution including nodal $\mathbf{K} = (\pi/2, \pi/2)$ and antinodal $\mathbf{K} = (\pi, 0)$ directions. Despite its accuracy, the relatively large $N_c = 16$ does not allow accessing low enough temperatures due to QMC sign problem so that some simulations using $N_c = 4$ provide further insights on the lowest temperature features in spite of the lack of the self-energy at the nodal direction. Fortunately, different N_c lead to quite similar results for high dopings (large ρ) and large ϵ_p. At lower dopings, however, it is not the case anymore so that adopting small $N_c = 4$ can lead to deviations from the physical reality and require more careful examination.

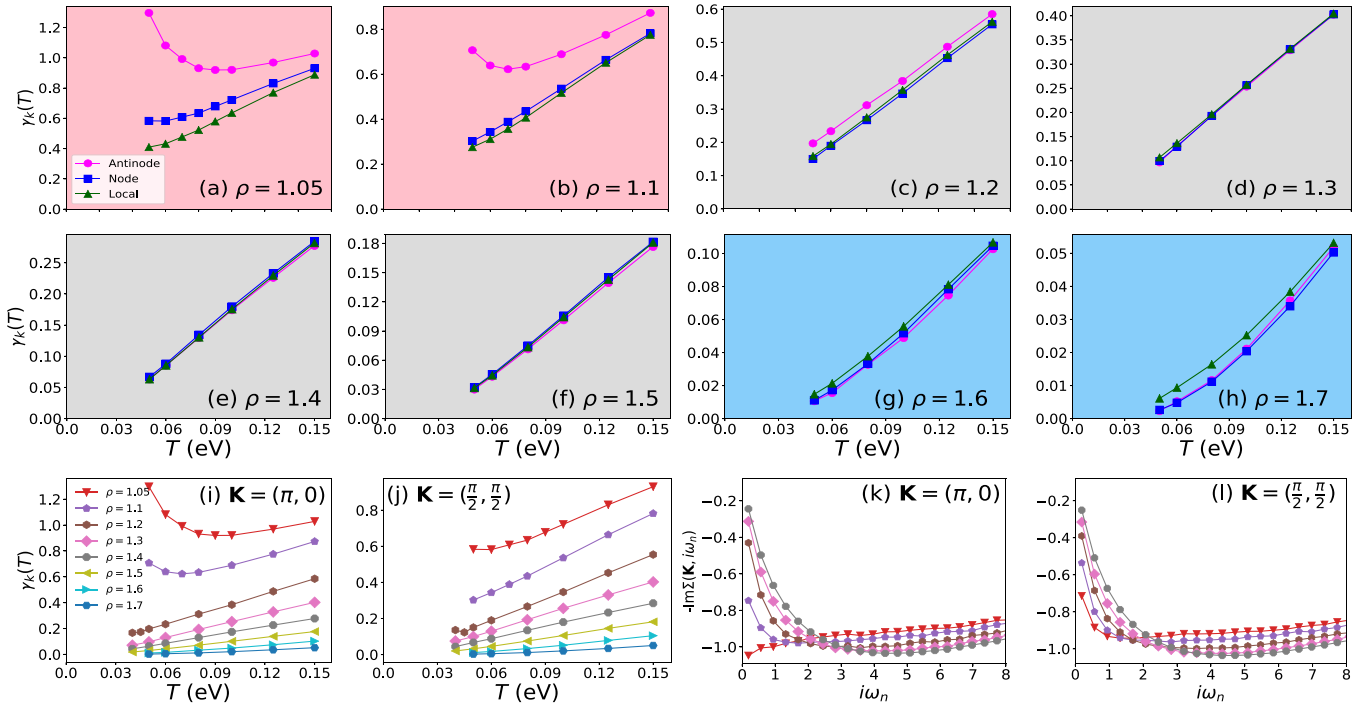

FIG. 1. (a)–(h) Temperature dependence of the electronic local scattering rate Γ and momentum-resolved γ_k at nodal $(\pi/2, \pi/2)$ and antinodal $(\pi, 0)$ directions for various density at $\epsilon_p = 3.24$ relevant to cuprates; (i)–(j) Comparison of γ_k with varying densities; (k)–(l) Frequency dependence of $-\mathrm{Im}\Sigma(\mathbf{K}, i\omega_n)$ for different densities at $T = 0.06$.

Another aspect is the momentum differentiation of the scattering rate, namely the deviation between nodal and antinodal directions, which is conventionally associated with the pseudogap (PG) features [23]. It is also valuable to explore the local scattering rate Γ as the momentum average of γ_k [24]. We believe that this is worthwhile even in the anisotropic situations to explore the difference between momentum averaged scattering rate and the values for a particular $\mathbf{K}$ direction. Throughout this work, we focus on the temperature evolution of Γ and γ_k for various hole density ρ per unit cell. Note that $\rho = 1$ corresponds to the half-filled system and $\rho > 1$ measures the hole doping. Regarding the site energy ϵ_p, we do not restrict on the case with $\epsilon_p = 3.24$ eV specific to cuprates but extend it to larger value, e.g., $\epsilon_p \sim 6.0$ eV relevant to different compounds, e.g., nickelates [60–62] or physical situations. We mention that the lowest accessible temperature is $T = 0.02$ eV for $N_c = 4$ simulations, which corresponds to ∼230 K in reality. It is extremely challenging to get access to even lower temperatures in various finite-temperature many-body simulations normally due to the negative fermionic sign problem.

III. RESULTS

A. $\epsilon_p = 3.24$ eV for cuprates

Figure 1 illustrates the temperature dependence of local scattering rate Γ as well as momentum-resolved γ_k of d orbital for varying density ρ at $\epsilon_p = 3.24$ relevant to cuprates. At small $\rho = 1.05$ (small hole doping) in panel (a), both the nodal and antinodal γ_k show a prominent upturn at low temperatures indicating the insulating behavior due to its closeness to the charge-transfer insulator at half-filling $\rho = 1.0$. This trend changes to the typical pseudogap (PS) feature akin to the single-band model [23], which is manifested by the observation that only the antinodal γ_k shows the upturn while the nodal γ_k remains its monotonic evolution until lowest simulated temperature, for instance, as shown in panel (b).

As the doping becomes progressively heavier (when ρ reaches 1.2 or higher), the linear-T dependence of γ_k at both directions extend to $T \to 0$. Our simulation indicate that the slope of $\gamma_k(T)$ at two directions are almost the same in a wide range of densities as evidenced in Fig. 1, panels (c)–(f). Interestingly, further hole doping at $\rho > 1.25$ leads to the nearly isotropic $\gamma_k(T)$, namely independent on the $\mathbf{K}$ direction. This is evidenced by the overlap of the local scattering rate $\Gamma(T)$ with the momentum-resolved $\gamma_k(T)$ for intermediate density range as shown in panels (d)–(f). The finding of this rather isotropic scattering rate might have connection with previous theoretical proposal relating the non-Fermi liquid and bad-metal physics to local spin fluctuations [22,70]. The panels (d)–(f) also show that the linear-in-T scattering rate persists for quite a wide density regime around $\rho \sim 1.2 - 1.5$, which extends to heavily doped side. Only at even higher density $\rho > 1.5$, $\gamma_k(T)$ deviates from the linear evolution at low temperatures. Note that in fact we cannot determine the physical behavior of $\gamma_k(T)$ at even lower temperatures, where the evolution can change in a qualitative manner. One additional interesting feature lies in the behavior of the local scattering rate Γ at high density, where it deviates from the overlapped γ_k of nodal and antinodal directions, which arises from the slightly different behavior at other directions, e.g., $\mathbf{K} = (0, 0), (\pi, \pi)$. Therefore, the truly isotropic scattering rate only applies for the intermediate density regime.

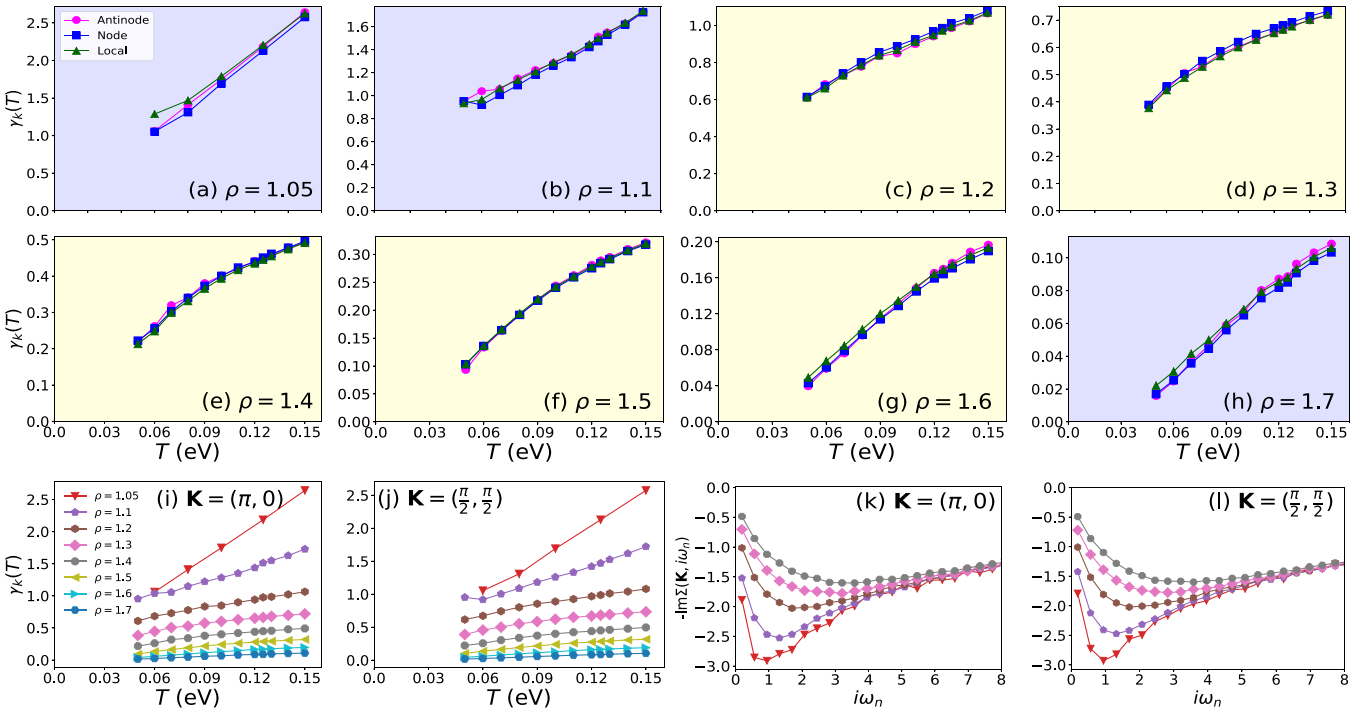

FIG. 2. Temperature dependence of the electronic local scattering rate Γ and momentum-resolved γ_k at nodal $(\pi/2, \pi/2)$ and antinodal $(\pi, 0)$ akin to Fig. 1 while at $\epsilon_p = 6.0$, presumably relevant to nickelates.

The caveat here is that physically the scattering rate should remain non-negative. Nonetheless, the interception of the linear fit (extrapolating γ_k to zero via $\gamma_k \sim aT + b$) leads to a nonphysical $\gamma_k(T = 0) < 0$. In fact, our simulated curves all show quite small positive or even negative $\gamma_k(T = 0)$. Hence, higher-order corrections such as quadratic evolution might develop in γ_k at lower T as the indication of the onset of Fermi-liquid physics or more complicated NFL features. Unfortunately, our simulations are limited by the severe sign problem for large enough N_c so that the physics at $T \to 0$ is not accessible at least for DCA simulations. As discussed previously in the literature [23,24], it is not appropriate to directly designate the observed behavior as the strange metal in these cases.

More detailed comparison between various situations are displayed in the bottom row of Fig. 1. The left two panels provide evidence that the slope of linear-T scattering rate $\gamma_k(T)$ decreases monotonically with increasing density. In fact, the scale of $\gamma_k(T)$ is already quite small at $\rho = 1.5$, indicating the strong metallic nature owing to the heavily doped charge carriers, in spite of its linear-T behavior. For completeness, the bottom right two panels give the frequency dependence of the self-energy, where the scattering rate $\gamma_k(T)$ is extracted. The transition from the low-density momentum differentiation to high-density isotropy is obvious.

B. $\epsilon_p = 6.0$ eV for nickelates

As mentioned before, our study does not restrict on the parameter sets relevant to cuprates. Figure 2 demonstrates the same scattering rates and frequency-dependent self-energy with only different $\epsilon_p = 6.0$ eV closely related to the recently discovered nickelate SC [60,62].

Firstly, the distinction from the $\epsilon_p = 3.24$ situation is that, at the same density, γ_k is globally larger than the values for $\epsilon_p = 3.24$, indicating stronger interaction effects. Note that our model does not include the explicit U_{pp} (to avoid the severe sign problem but its role needs further exploration) so that the sole player governing the electronic interaction seems originating from U_{dd} while it normally leads to momentum differentiation, whose absence in our simulations prompts additional reasons for the observed larger scattering rates. Physically, the large ϵ_p discourages the charge carriers locating onto the p orbitals so that the effectively more carrier density on d orbital induces stronger interaction effects from U_{dd}. The charge redistribution with different ϵ_p can be clearly seen in Fig. 3, where the larger $\epsilon_p = 6.0$ promotes more hole

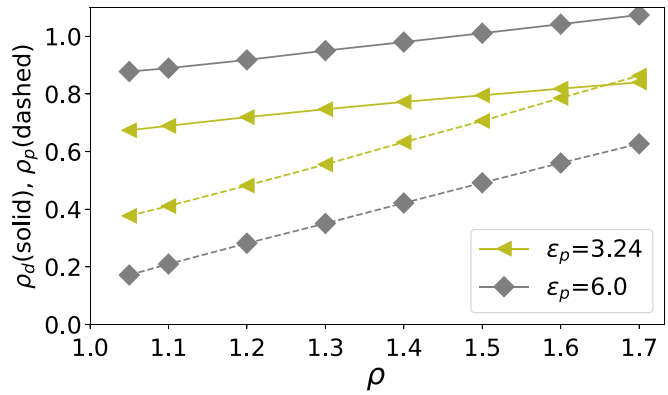

FIG. 3. Evolution of charge distribution with total density ρ. Larger $\epsilon_p = 6.0$ promotes more hole occupancy on d orbital compared to $\epsilon_p = 3.24$ while suppresses ρ_p.

occupancy on d orbital compared to $\epsilon_p = 3.24$ while suppresses ρ_p. Note also the comparison of the increasing rate of $\rho_d(\rho)$ versus $\rho_p(\rho)$ for two different ϵ_p.

Secondly, γ_k is almost isotropic with respect to $\mathbf{K}$ regardless of the density except for very low hole doping $\rho = 1.05$ in panel (a). This is further evidenced by the overlap between the local scattering rate Γ and the momentum-resolved γ_k in most cases. As discussed before, the reduced hopping through the oxygens due to higher ϵ_p leads to stronger effective U_{dd}. Indeed, previous studies on the single-band Hubbard model revealed that the momentum-selective behavior (pseudogap physics) does not persist for large enough Hubbard U [71], which is consistent with the isotropy discovered here. Owing to this observation, it is plausible to examine the fate of γ_k at lower temperature by adopting smaller $N_c = 4$ DCA cluster, which will be discussed later.

The most prominent feature for $\epsilon_p = 6.0$ is that the linear-T dependence of γ_k occurs only for a limited temperature interval at small density like $\rho = 1.05$ in panel (a) or large density $\rho = 1.7$ in panel (h) in spite of the extrapolated negative interception at $T = 0$. In contrast, for intermediate densities, γ_k exhibits a downturn as the temperature decreases as shown in panels (c)–(g). This phenomena is reminiscent of the recent findings of T-linear scattering for single-band Hubbard model on triangular lattice that is claimed to originate from two distinct mechanisms, namely the metal-to-pseudogap transition at low doping and solely interaction-driven at high dopings [24]. Its connection with our findings here is unclear and may deserve further exploration. Note that our observed downturn starts from a slightly higher temperature scale $T \sim 0.1$.

Akin to Fig 1, the two left bottom panels provide summarized comparison between γ_k at the antinodal and nodal directions. The trend of decreasing scattering rate with hole doping is apparently similar to the situations for $\epsilon_p = 3.24$. The two right bottom panels vividly show the isotropy of the self-energy in systems of large $\epsilon_p = 6.0$.

C. Downturn of γ_k at large ϵ_p

The intriguing downturn features motivate us to further explore the associated physics at lower temperatures. Whereas the effectively stronger interaction effects for larger $\epsilon_p = 6.0$ do not allow us to get access to lower temperatures, the isotropy of the scattering rate revealed in Fig. 2 fortunately permits adopting smaller DCA cluster like $N_c = 4$ to partly alleviate the QMC sign problem for simulating lower T systems.

Figure 4 compares the results of γ_k at antinodal direction between $N_c = 4$ and $N_c = 16$, which generically display quantitative deviation except for high density, e.g., $\rho = 1.7$. It can be seen that the dominant feature is the two consecutive nearly linear-T regimes of antinodal γ_k connected via a smooth crossover around $T \sim 0.08$ for intermediate densities as shown in panels (c)–(g). Nonetheless, this feature is only obvious for $N_c = 4$ simulations while larger $N_c = 16$ seemingly smooths these out so that might question the physical reality of this phenomenology in the Emery model.

Physically, this is reminiscent of the recent experimental demonstration of the crossovers between different

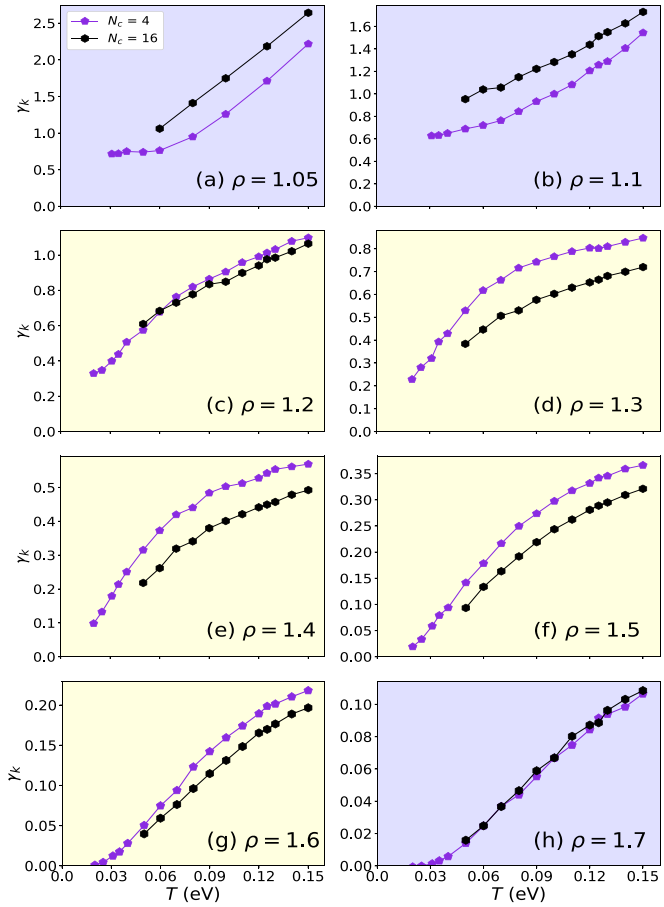

FIG. 4. Comparison of antinodal scattering rate γ_k between $N_c = 4, 16$ simulations for $\epsilon_p = 6.0$. The curves at lower temperature reveal additional features unavailable in large $N_c = 16$ simulations.

temperature regimes signaling the Fermi liquid (FL), strange metal (SM), and empirical high-temperature bad-metal state (similar to the strange metal but does not host well-defined quasiparticle) [72]. In fact, the earlier theoretical calculations based on large-U Hubbard and t-J models have uncovered similar behavior [26,73–75]. At the lowest temperature, the resistivity is typically proportional to T^2 as a FL. Increasing temperature induces the linear resistivity indicating the SM regime. At even higher temperatures, the system enters into a bad-metal regime with a different slope of the linear-T resistivity.

Apart from the feature of two linear-T regimes, the low-density limit shows saturated scattering rate, which cannot be seen at large $N_c = 16$ simulations. This again implies the intrinsically strong interaction effects arising from large $\epsilon_p = 6.0$. In contrast, at high density $\rho = 1.7$, the perfect agreement between $N_c = 4, 16$ at high temperatures provides evidence on the crossover to the apparent T^2 behavior seen for $N_c = 4$ curve at lower temperatures. This $N_c = 4$ simulation complements our understanding of ultimate fate of the linear-T scattering rate with an unphysical negative interception extrapolated to $T = 0$.

In addition to the two characteristic values of $\epsilon_p = 3.24$ and 6.0, Fig. 5 provides more information on the ϵ_p dependence of the scattering rate. Here, the deviation between

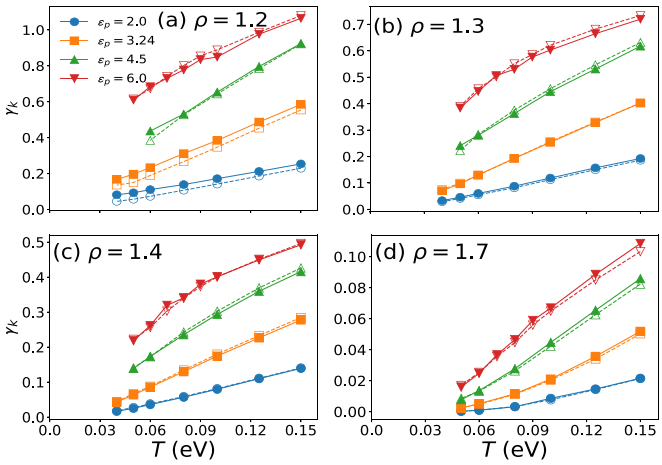

FIG. 5. ϵ_p dependence of the electronic scattering rate γ_k at antinodal (solid) and nodal (dashed) directions, whose downturn occurs for relatively large $\epsilon_p = 4.5, 6.0$ at intermediate densities of panels (b)–(c). The increase of ϵ_p generically leads to larger scattering rate reflecting stronger interaction effects.

antinodal (solid) and nodal (dashed) γ_k is mostly dominant at smaller density like $\rho = 1.2$ while can be neglected at larger densities. Apparently, the downturn of γ_k occurs only for relatively large $\epsilon_p = 4.5, 6.0$ at intermediate density, e.g., $\rho = 1.3, 1.4$ in panels (b)–(c). It is naturally expected that the downturn folding might be even more obvious at larger $\epsilon_p > 6.0$ while the temperature scale is always around $T \sim 0.1$.

Undoubtedly, Fig. 5 also illustrates that the increase of ϵ_p generically leads to higher scale of the scattering rate, which matches with the physical expectation that larger ϵ_p promotes higher carrier density on d orbital so that effectively induces stronger interaction effects. Interestingly, if naively assuming the T^α dependence of γ_k, panel (d) at large density $\rho = 1.7$ vividly displays the gradual crossover from the $\alpha > 1$ at small $\epsilon_p = 2.0$ to $\alpha < 1$ (downturn) at large $\epsilon_p = 6.0$.

D. Quasiparticle weight and scattering rate

In the presence of electronic interaction, it is worthwhile further investigating the quasiparticle scattering rate or inverse quasiparticle lifetime $1/\tau_k = Z_k\gamma_k$, which differs from the electronic scattering rate γ_k by the so-called quasiparticle weight Z_k. The consideration of the quasipariticle scattering rate is essential to account for the many-body interaction effects within strongly correlated systems and is also more closely related to the experimental transport properties than the single-particle electronic scattering rate γ_k discussed earlier [76]. As mentioned earlier, note that the quasiparticle picture can even break down in the strange metal, which is still an unresolved open problem [67–69]. Here our adopted conventional quasiparticle picture can still provide some insight on the properties of the Emery model.

Numerically, Z_k can be approximately evaluated [24] by

$$Z_k \approx \left[1 - \frac{\Im\Sigma(i\omega_0)}{\omega_0}\right]^{-1}. \quad (2)$$

One prediction of the Planckian dissipation theory [3,11,12] is that the inverse quasiparticle lifetime $1/\tau_k$ is proportional to absolute temperature T with a coefficient close to unity [3,11,12], which is found to be quantitatively incompatible with the previous numerical studies on single-band model on square [23] and triangular lattice [24].

Figure 6 demonstrates that this prediction of unity slope only crudely holds true for $\rho \sim 1.4$ at $\epsilon_p = 3.24$ and for $\rho \sim 1.5$ at $\epsilon_p = 6.0$ (note that the black dashed line has unity slope for reference). In this sense, we have not found any decisive signature for the unity slope feature associated with the universal Planckian limit. Apart from the slope, the general trend of the quasiparticle scattering rate in terms of the density is similar to the electronic scattering rate γ_k for both nodal and antinodal directions. Besides, the bottom panels show that there also exists the downturn of $1/\tau_k$ at temperatures below $T \sim 0.1$ for intermediate densities, which matches with the behavior of γ_k generically.

Figure 6 also displays the quasiparticle weight Z_k that is capable to characterize its closeness to conventional Fermi liquid (with $Z_k = 1$). Undoubtedly, Z_k increases with the density reflecting the role of doped holes. Additionally, it is always weakly temperature dependent or even independent except for the low doping $\rho = 1.05, 1.1$ at $\epsilon_p = 3.24$, which is normally associated with their PG features.

IV. SUMMARY AND OUTLOOK

In summary, motivated by the numerical exploration of the non-Fermi-liquid signatures in the single-band Hubbard model [23,24], we have employed the dynamic cluster quantum Monte Carlo calculations to systematically investigate the temperature dependence of the electronic and quasiparticle scattering rates in the framework of two-dimensional three-orbital Emery model, which is generically believed to capture the physics of cuprate SC more accurately [23,51,52].

Our numerical simulations reveal that the systems with moderate site energy of p-orbital $\epsilon_p = 3.24$ relevant to cuprates support the linear-in-T scattering rates for a range of intermediate densities $\rho = 1.2 - 1.5$, while the small densities feature PG behavior and large densities show the conventional Fermi liquid characterized by T^2 scattering rates. Nonetheless, in many cases, the interception at $T = 0$ is negative, indicating that other factors have to be included to account for the physical reality.

Our study also extends to the relatively large $\epsilon_p = 6.0$, presumably relevant to newly discovered nickelate SC. For these systems, the common feature lies in the downturn of the scattering rate below the temperature scale $T \sim 0.1$. Our simulations at smaller DCA cluster $N_c = 4$, which is reasonable owing to the isotropy of the scattering rate, confirms this observation by revealing two consecutive linear-T regimes of γ_k. More simulations on other ϵ_p values provide further evidence that only relatively large ϵ_p would induce such a downturn of γ_k. To have a complete understanding of the many-body effects, we also illustrated the behavior of quasiparticle scattering rate, which generically departs from the unity slope as the prediction of Planckian dissipation theory. The quasiparticle weight is monotonically increasing with the

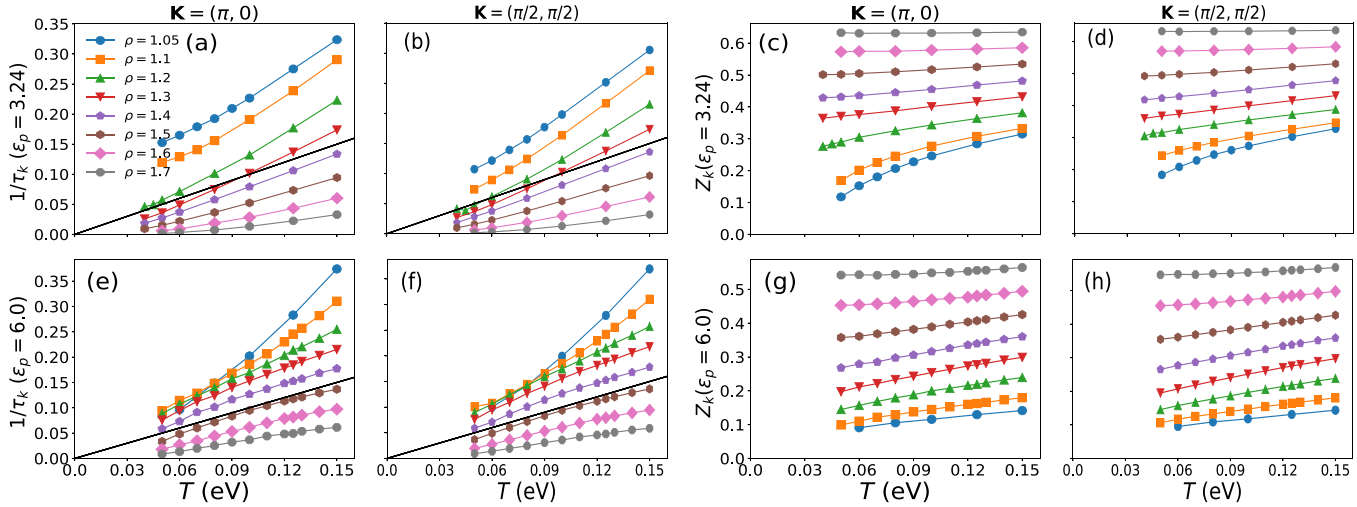

FIG. 6. Temperature dependence of the momentum-resolved quasiparticle scattering rate $1/\tau_k$ and quasiparticle weight Z_k at nodal $(\pi/2, \pi/2)$ and antinodal $(\pi, 0)$ directions for various density at (Upper) $\epsilon_p = 3.24$ and (Lower) $\epsilon_p = 6.0$.

hole density as expected owing to the enhanced metallicity from the doped charge carriers.

Overall, our numerical findings of the three-orbital Emery model generally match with those observed in two-dimensional Hubbard model [23]. The hole doping/density range of NFL state is very narrow. Hindered by the negative sign problem, however, we are unable to definitively identify the doping range exhibiting perfect linear-in-temperature behavior in large enough DCA cluster. Our presented work provides quantitative examination of linear-T features of the scattering rates in the celebrated Emery model.

Because our current investigation only focused on the scattering rate but neglected other closely related physics such as SC and magnetic/charge ordering, some further directions deserve future exploration. For instance, the most recent transport experiments have revealed some relations between the superconducting T_c and the strange metal's slope A as $T_c \sim \sqrt{A}$ in the cuprate SC [77]. The detailed studies on the connection between SC and the behavior of scattering rate would be interesting. Besides, despite that relatively large ϵ_p might be detrimental to SC [52], it can be fruitful to find other physical quantities having decisive relation with the behavior associated with the scattering rate uncovered in the present work. Another direction might be more investigation on the high hole or electron doping systems since our current study at large hole density $\rho = 1.7$ has demonstrated interesting linear-T behavior of the scattering rate.

In addition, in light of the most recent experimental demonstration of the cupratelike electronic structure of infinite-layer nickelates [53,54] revealing the dominant role of $d_{x^2-y^2}$ orbital and the previous evidence of the large charge-transfer energy in these nickelates, our current investigation of the Emery model at relatively large ϵ_p would provide particularly important information on the nickelates. This exploration sheds light on some fundamental factors governing the physics of nickelates and cuprates. However, it is still questionable that whether the uncovered three-dimensional (3D) electron pocket centered at Brillouin zone corner originating from the rare-earth atoms of the nickelates plays the vital or only marginal roles.

ACKNOWLEDGMENTS

We would like to thank Wenxin Ding, Wei Wu, and Peizhi Mai for illuminating discussions in the early stage. We acknowledge the support by National Natural Science Foundation of China (NSFC) Grant No. 12174278, startup fund from Soochow University, and Priority Academic Program Development (PAPD) of Jiangsu Higher Education Institutions.

[1] G. Stewart, Non-Fermi-liquid behavior in d- and f- electron metals, Rev. Mod. Phys. **73**, 797 (2001).

[2] R. L. Greene, P. R. Mandal, N. R. Poniatowski, and T. Sarkar, The strange metal state of the electron-doped cuprates, Annu. Rev. Condens. Matter Phys. **11**, 213 (2020).

[3] S. A. Hartnoll and A. P. Mackenzie, Colloquium: Planckian dissipation in metals, Rev. Mod. Phys. **94**, 041002 (2022).

[4] C. M. Varma, Colloquium: Linear in temperature resistivity and associated mysteries including high temperature superconductivity, Rev. Mod. Phys. **92**, 031001 (2020).

[5] Y. Cao, D. Chowdhury, D. Rodan-Legrain, O. Rubies-Bigorda, K. Watanabe, T. Taniguchi, T. Senthil, and P. Jarillo-Herrero, Strange metal in magic-angle graphene with near Planckian dissipation, Phys. Rev. Lett. **124**, 076801 (2020).

[6] N. Doiron-Leyraud, P. Auban-Senzier, S. R. de Cotret, C. Bourbonnais, D. Jérome, K. Bechgaard, and L. Taillefer, Correlation between linear resistivity and T_c in the Bechgaard salts and the pnictide superconductor $Ba(Fe_{1-x}Co_x)_2As_2$, Phys. Rev. B **80**, 214531 (2009).

[7] J. Custers, P. Gegenwart, H. Wilhelm, K. Neumaier, Y. Tokiwa, O. Trovarelli, C. Geibel, F. Steglich, C. Pépin, and P. Coleman, The break-up of heavy electrons at a quantum critical point, Nature (London) **424**, 524 (2003).

[8] J. Ayres, M. Berben, M. Čulo, Y.-T. Hsu, E. van Heumen, Y. Huang, J. Zaanen, T. Kondo, T. Takeuchi, J. Cooper *et al.*, Incoherent transport across the strange-metal regime of overdoped cuprates, Nature (London) **595**, 661 (2021).

[9] R. A. Cooper, Y. Wang, B. Vignolle, O. Lipscombe, S. M. Hayden, Y. Tanabe, T. Adachi, Y. Koike, M. Nohara, H. Takagi *et al.*, Anomalous criticality in the electrical resistivity of $La_{2-x}Sr_xCuO_4$, Science **323**, 603 (2009).

[10] R. Daou, N. Doiron-Leyraud, D. LeBoeuf, S. Li, F. Laliberté, O. Cyr-Choiniere, Y. Jo, L. Balicas, J.-Q. Yan, J.-S. Zhou *et al.*, Linear temperature dependence of resistivity and change in the Fermi surface at the pseudogap critical point of a high-T_c superconductor, Nat. Phys. **5**, 31 (2009).

[11] J. Zaanen, Why the temperature is high, Nature (London) **430**, 512 (2004).

[12] J. Zaanen, Planckian dissipation, minimal viscosity and the transport in cuprate strange metals, SciPost Phys. **6**, 061 (2019).

[13] C. H. Mousatov, I. Esterlis, and S. A. Hartnoll, Bad metallic transport in a modified Hubbard model, Phys. Rev. Lett. **122**, 186601 (2019).

[14] M. Sentef, P. Werner, E. Gull, and A. P. Kampf, Superconducting phase and pairing fluctuations in the half-filled two-dimensional Hubbard model, Phys. Rev. Lett. **107**, 126401 (2011).

[15] V. Zlatić, G. Boyd, and J. K. Freericks, Universal thermopower of bad metals, Phys. Rev. B **89**, 155101 (2014).

[16] J. A. Riera and E. Dagotto, Optical conductivity of the Hubbard model at finite temperature, Phys. Rev. B **50**, 452 (1994).

[17] N. Pakhira and R. H. McKenzie, Absence of a quantum limit to charge diffusion in bad metals, Phys. Rev. B **91**, 075124 (2015).

[18] T. Dahm, L. Tewordt, and S. Wermbter, Self-consistent calculation of physical quantities for the two-dimensional Hubbard model and comparison with cuprate high-T_c superconductors, J. Low Temp. Phys. **96**, 275 (1994).

[19] A. Vranić, J. Vučičević, J. Kokalj, J. Skolimowski, R. Žitko, J. Mravlje, and D. Tanasković, Charge transport in the Hubbard model at high temperatures: Triangular versus square lattice, Phys. Rev. B **102**, 115142 (2020).

[20] P. Cha, N. Wentzell, O. Parcollet, A. Georges, and E.-A. Kim, Linear resistivity and Sachdev-Ye-Kitaev (SYK) spin liquid behavior in a quantum critical metal with spin-1/2 fermions, Proc. Natl. Acad. Sci. USA **117**, 18341 (2020).

[21] E. Berg, S. Lederer, Y. Schattner, and S. Trebst, Monte Carlo studies of quantum critical metals, Annu. Rev. Condens. Matter Phys. **10**, 63 (2019).

[22] P. Werner, S. Hoshino, and H. Shinaoka, Spin-freezing perspective on cuprates, Phys. Rev. B **94**, 245134 (2016).

[23] W. Wú, X. Wang, and A.-M. Tremblay, Non-Fermi liquid phase and linear-in-temperature scattering rate in overdoped two-dimensional Hubbard model, Proc. Natl. Acad. Sci. USA **119**, e2115819119 (2022).

[24] J. Fournier, P.-O. Downey, C.-D. Hébert, M. Charlebois, and A. Tremblay, Two T-linear scattering rate regimes in the triangular lattice Hubbard model, arXiv:2312.08306.

[25] A. D. Arulsamy, Origin of strange metallic phase in cuprate superconductors, J. Supercond. Novel Magn. **27**, 309 (2014).

[26] W. Ding, R. Zitko, P. Mai, E. Perepelitsky, and B. S. Shastry, Strange metal from Gutzwiller correlations in infinite dimensions, Phys. Rev. B **96**, 054114 (2017).

[27] P. Phillips, Mottness collapse and T-linear resistivity in cuprate superconductors, Philos. Trans. R. Soc. A **369**, 1574 (2011).

[28] T. G. Kiely and E. J. Mueller, Transport in the two-dimensional Fermi-Hubbard model: Lessons from weak coupling, Phys. Rev. B **104**, 165143 (2021).

[29] A. A. Patel and H. J. Changlani, Many-body energy invariant for T-linear resistivity, Phys. Rev. B **105**, L201108 (2022).

[30] H. C. Kao, D. Li, and B. Rosenstein, Unified intermediate coupling description of pseudogap and strange metal phases of cuprates, Phys. Rev. B **107**, 054508 (2023).

[31] W. Xu, W. McGehee, W. Morong, and B. DeMarco, Bad-metal relaxation dynamics in a Fermi lattice gas, Nat. Commun. **10**, 1588 (2019).

[32] J. Zaanen, G. A. Sawatzky, and J. W. Allen, Band gaps and electronic structure of transition-metal compounds, Phys. Rev. Lett. **55**, 418 (1985).

[33] H. Xu, C.-M. Chung, M. Qin, U. Schollwöck, S. R. White, and S. Zhang, Coexistence of superconductivity with partially filled stripes in the Hubbard model, arXiv:2303.08376.

[34] Y.-F. Jiang, T. P. Devereaux, and H.-C. Jiang, Ground-state phase diagram and superconductivity of the doped Hubbard model on six-leg square cylinders, Phys. Rev. B **109**, 085121 (2024).

[35] A. Lechiara, V. Marino, and L. F. Tocchio, Variational Monte Carlo study of stripes as a function of doping in the $t-t'$ Hubbard model, arXiv:2403.02073.

[36] V. Emery, Theory of high-T_c superconductivity in oxides, Phys. Rev. Lett. **58**, 2794 (1987).

[37] H.-C. Jiang, Pair density wave in the doped three-band Hubbard model on two-leg square cylinders, Phys. Rev. B **107**, 214504 (2023).

[38] A. Chiciak, E. Vitali, and S. Zhang, Magnetic and charge orders in the ground state of the Emery model: Accurate numerical results, Phys. Rev. B **102**, 214512 (2020).

[39] S. R. White and D. J. Scalapino, Doping asymmetry and striping in a three-orbital CuO_2 Hubbard model, Phys. Rev. B **92**, 205112 (2015).

[40] P. Mai, G. Balduzzi, S. Johnston, and T. A. Maier, Orbital structure of the effective pairing interaction in the high-temperature superconducting cuprates, npj Quantum Mater. **6**, 26 (2021).

[41] L. de'Medici, X. Wang, M. Capone, and A. J. Millis, Correlation strength, gaps, and particle-hole asymmetry in high-T_c cuprates: A dynamical mean field study of the three-band copper-oxide model, Phys. Rev. B **80**, 054501 (2009).

[42] M. Guerrero, J. E. Gubernatis, and S. Zhang, Quantum Monte Carlo study of hole binding and pairing correlations in the three-band Hubbard model, Phys. Rev. B **57**, 11980 (1998).

[43] R. T. Scalettar, D. J. Scalapino, R. L. Sugar, and S. R. White, Antiferromagnetic, charge-transfer, and pairing

correlations in the three-band Hubbard model, Phys. Rev. B **44**, 770 (1991).

[44] P. R. C. Kent, T. Saha-Dasgupta, O. Jepsen, O. K. Andersen, A. Macridin, T. A. Maier, M. Jarrell, and T. C. Schulthess, Combined density functional and dynamical cluster quantum Monte Carlo calculations of the three-band Hubbard model for hole-doped cuprate superconductors, Phys. Rev. B **78**, 035132 (2008).

[45] K. Sheshadri, D. Malterre, A. Fujimori, and A. Chainani, Connecting the one-band and three-band Hubbard models of cuprates via spectroscopy and scattering experiments, Phys. Rev. B **107**, 085125 (2023).

[46] B. Ponsioen, S. S. Chung, and P. Corboz, Superconducting stripes in the hole-doped three-band Hubbard model, Phys. Rev. B **108**, 205154 (2023).

[47] E. Vitali, H. Shi, A. Chiciak, and S. Zhang, Metal-insulator transition in the ground state of the three-band Hubbard model at half filling, Phys. Rev. B **99**, 165116 (2019).

[48] S. Jiang, D. J. Scalapino, and S. R. White, Density matrix renormalization group based downfolding of the three-band Hubbard model: Importance of density-assisted hopping, Phys. Rev. B **108**, L161111 (2023).

[49] Z.-H. Cui, C. Sun, U. Ray, B.-X. Zheng, Q. Sun, and G. K.-L. Chan, Ground-state phase diagram of the three-band Hubbard model from density matrix embedding theory, Phys. Rev. Res. **2**, 043259 (2020).

[50] S. Jiang, D. J. Scalapino, and S. R. White, A single-band model with enhanced pairing from DMRG-based downfolding of the three-band Hubbard model, arXiv:2303.00756.

[51] Y. Kung, C.-C. Chen, Y. Wang, E. Huang, E. Nowadnick, B. Moritz, R. Scalettar, S. Johnston, and T. Devereaux, Characterizing the three-orbital Hubbard model with determinant quantum Monte Carlo, Phys. Rev. B **93**, 155166 (2016).

[52] P. Mai, G. Balduzzi, S. Johnston, and T. A. Maier, Pairing correlations in the cuprates: A numerical study of the three-band Hubbard model, Phys. Rev. B **103**, 144514 (2021).

[53] X. Ding, Y. Fan, X. X. Wang, C. H. Li, Z. T. An, J. H. Ye, S. L. Tang, M. Y. N. Lei, X. T. Sun, N. Guo, Z. H. Chen, S. Sangphet, Y. L. Wang, H. C. Xu, R. Peng, and D. L. Feng, Cuprate-like electronic structures in infinite-layer nickelates with 3D dispersion, arXiv:2403.07448.

[54] W. Sun, Z. Jiang, C. Xia, B. Hao, Y. Li, S. Yan, M. Wang, H. Liu, J. Ding, J. Liu, Z. Liu, J. Liu, H. Chen, D. Shen, and Y. Nie, Electronic structure of superconducting infinite-layer lanthanum nickelates, arXiv:2403.07344.

[55] D. Li, K. Lee, B. Y. Wang, M. Osada, S. Crossley, H. R. Lee, Y. Cui, Y. Hikita, and H. Y. Hwang, Superconductivity in an infinite-layer nickelate, Nature (London) **572**, 624 (2019).

[56] M. Osada, B. Y. Wang, K. Lee, D. Li, and H. Y. Hwang, Phase diagram of infinite layer praseodymium nickelate $Pr_{1-x}Sr_xNiO_2$ thin films, Phys. Rev. Mater. **4**, 121801(R) (2020).

[57] M. Osada, B. Y. Wang, B. H. Goodge, S. P. Harvey, K. Lee, D. Li, L. F. Kourkoutis, and H. Y. Hwang, Nickelate superconductivity without rare-earth magnetism:$(La, Sr)NiO_2$, Adv. Mater. **33**, 2104083 (2021).

[58] S. Zeng, C. Li, L. E. Chow, Y. Cao, Z. Zhang, C. S. Tang, X. Yin, Z. S. Lim, J. Hu, P. Yang *et al.*, Superconductivity in infinite-layer nickelate $La_{1-x}Ca_xNiO_2$ thin films, Sci. Adv. **8**, eabl9927 (2022).

[59] G. A. Pan, D. Ferenc Segedin, H. LaBollita, Q. Song, E. M. Nica, B. H. Goodge, A. T. Pierce, S. Doyle, S. Novakov, D. Córdova Carrizales *et al.*, Superconductivity in a quintuple-layer square-planar nickelate, Nat. Mater. **21**, 160 (2022).

[60] M. Jiang, M. Berciu, and G. A. Sawatzky, Critical nature of the Ni spin state in doped $NdNiO_2$, Phys. Rev. Lett. **124**, 207004 (2020).

[61] Y. Nomura and R. Arita, Superconductivity in infinite-layer nickelates, Rep. Prog. Phys. **85**, 052501 (2022).

[62] A. S. Botana, F. Bernardini, and A. Cano, Nickelate superconductors: an ongoing dialog between theory and experiments, J. Exp. Theor. Phys. **132**, 618 (2021).

[63] M. H. Hettler, A. N. Tahvildar-Zadeh, M. Jarrell, T. Pruschke, and H. R. Krishnamurthy, Nonlocal dynamical correlations of strongly interacting electron systems, Phys. Rev. B **58**, R7475(R) (1998).

[64] T. Maier, M. Jarrell, T. Pruschke, and M. H. Hettler, Quantum cluster theories, Rev. Mod. Phys. **77**, 1027 (2005).

[65] U. R. Hähner, G. Alvarez, T. A. Maier, R. Solcà, P. Staar, M. S. Summers, and T. C. Schulthess, DCA++: A software framework to solve correlated electron problems with modern quantum cluster methods, Comput. Phys. Commun. **246**, 106709 (2020).

[66] E. Gull, P. Werner, O. Parcollet, and M. Troyer, Continuous-time auxiliary-field Monte Carlo for quantum impurity models, Europhys. Lett. **82**, 57003 (2008).

[67] D. Chowdhury, A. Georges, O. Parcollet, and S. Sachdev, Sachdev-Ye-Kitaev models and beyond: Window into non-Fermi liquids, Rev. Mod. Phys. **94**, 035004 (2022).

[68] P. W. Phillips, N. E. Hussey, and P. Abbamonte, Stranger than metals, Science **377**, eabh4273 (2022).

[69] H. Hu, L. Chen, and Q. Si, Quantum critical metals: Dynamical planckian scaling and loss of quasiparticles, arXiv:2210.14183.

[70] P. Werner, X. Chen, and E. Gull, Ferromagnetic spin correlations in the two-dimensional Hubbard model, Phys. Rev. Res. **2**, 023037 (2020).

[71] E. Gull, O. Parcollet, P. Werner, and A. J. Millis, Momentum-sector-selective metal-insulator transition in the eight-site dynamical mean-field approximation to the Hubbard model in two dimensions, Phys. Rev. B **80**, 245102 (2009).

[72] Y. Yang, Q. Tao, Y. Fang, G. Tang, C. Yao, X. Yan, C. Jiang, X. Xu, F. Huang, W. Ding *et al.*, Anomalous enhancement of the Nernst effect at the crossover between a Fermi liquid and a strange metal, Nat. Phys. **19**, 379 (2023).

[73] B. S. Shastry and E. Perepelitsky, Low-energy physics of the $t-J$ model in $d=\infty$ using extremely correlated Fermi liquid theory: Cutoff second-order equations, Phys. Rev. B **94**, 045138 (2016).

[74] E. Perepelitsky, A. Galatas, J. Mravlje, R. Zitko, E. Khatami, B. S. Shastry, and A. Georges, Transport and optical conductivity in the Hubbard model: A high-temperature expansion perspective, Phys. Rev. B **94**, 235115 (2016).

[75] B. S. Shastry and P. Mai, Aspects of the normal state resistivity of cuprate superconductors, Phys. Rev. B **101**, 115121 (2020).

[76] W. Nolting and W. D. Brewer, *Fundamentals of Many-Body Physics* (Springer, Berlin, Heidelberg, 2009).

[77] J. Yuan, Q. Chen, K. Jiang, Z. Feng, Z. Lin, H. Yu, G. He, J. Zhang, X. Jiang, X. Zhang *et al.*, Scaling of the strange-metal scattering in unconventional superconductors, Nature (London) **602**, 431 (2022).